



Microstructure evolution and mechanical properties of spark plasma sintered W–Ni–Mn alloy

Yan-lin PAN, Lei DING, Dao-ping XIANG

State Key Laboratory of Marine Resource Utilization in South China Sea,
Hainan University, Haikou 570228, China

Received 13 April 2016; accepted 26 September 2016

Abstract: Tungsten heavy alloys (90W–6Ni–4Mn) were prepared through spark plasma sintering (SPS) using micron-sized W, Ni, and Mn powders without ball milling as raw materials. The effects of sintering temperature on the microstructure and mechanical properties of the 90W–6Ni–4Mn alloys were investigated. SPS technology was used to prepare 90W–6Ni–4Mn alloys with relatively high density and excellent comprehensive performance at 1150–1250 °C for 3 min. The 90W–6Ni–4Mn alloys consisted of the W phase and the γ -(Ni, Mn, and W) binding phase, and the average grain size was less than 10 μm . The Rockwell hardness and bending strength of alloys first increased and then decreased with increasing sintering temperature. The best comprehensive performance was obtained at 1200 °C, its hardness and bending strength were HRA 68.7 and 1162.72 MPa, respectively.

Key words: 90W–6Ni–4Mn alloy; spark plasma sintering; microstructure; Rockwell hardness; bending strength

1 Introduction

Tungsten heavy alloys (WHAs) exhibiting good comprehensive performance, such as high density, high strength, good machinability, and an optimum thermal expansion coefficient; these alloys are extensively applied in the national defense, military, and aviation fields [1,2]. To date, the main materials used for kinetic energy penetrators are depleted uranium (DU) and WHAs. A DU warhead has better penetration depth but can severely pollute the environment [3]. The current WHA warheads commonly use the W–Ni–Fe alloy. However, the W–Ni–Fe alloys are not so sensitive to adiabatic shear band. Consequently, the warhead easily forms a mushroom head during the armor-piercing process, thereby leading to the 8%–10% decrease in penetration capability. W–Ni–Mn alloys have recently attracted attention. Compared with the W–Ni–Fe alloys, the W–Ni–Mn alloys have good adiabatic shear performance and exhibit a self-sharpening performance during the armor-piercing process [4], thereby avoiding a decrease in the penetration depth; thus, this alloy is a potential substitute for DU materials.

For the W–Ni–Mn alloys, the oxidation of Mn, the growth of W grains, and the volatilization of the binding phase restrict the significant improvement of the alloy performance during the sintering process. The W–Ni–Mn alloys are usually prepared by traditional liquid phase sintering method. ZAHRAEE et al [5] have investigated the Mn/Ni ratio variation on the microstructure of W–Ni–Mn alloy, and LIU et al [6] and CHEN et al [7] examined the processing parameters on the microstructure and mechanical properties of W–Ni–Mn alloy. In previous studies, a high sintering temperature can lead to a large W grain size. Meanwhile, Mn is easily oxidized during the sintering process, resulting in low density and limited mechanical properties. Compared with the conventional liquid phase sintering method, the spark plasma sintering (SPS) technique is a new sintering technology with several advantages, lower sintering temperature since pressure applied simultaneously, and short sintering time. The SPS technique is extensively used for preparing W–Ni–Cu [8] and W–Ni–Fe [9,10] alloys. However, studies have not been reported on the microstructure and mechanical properties of the W–Ni–Mn alloy prepared by the SPS technique to our knowledge. In the present

study, the 90W–6Ni–4Mn alloys were prepared by the SPS technique from micron-sized W, Ni, and Mn powders without ball milling as raw materials. The microstructure and mechanical properties of 90W–6Ni–4Mn alloys were investigated. Our results can be used as the experimental and theoretical bases for the application of the W–Ni–Mn alloy warhead.

2 Experimental

The raw materials were reduced tungsten powder, carbonyl nickel powder, and electrolytic manganese powder (>99.5% purity). The average particle size was approximately 4 μm for W powder, 1 μm for Ni powder, and 2.8 μm for Mn powder. The mass ratio of W–Ni–Mn was 90:6:4. Known amounts of the raw materials were weighed, placed in a stainless steel jar, and mixed without milling media for 20 h with Ar protection in a QM-QX planetary ball mill to obtain a mixed raw material powder with the 340 r/min rotating speed, the morphology of the blended powders was shown in Fig. 1. The LABOXTM-3010K spark plasma sintering system was used to prepare the 90W–6Ni–4Mn alloy. The composite powders were sintered in the SPS system for 3 min at a pressure of 30 MPa, a temperature of 1050 to 1300 $^{\circ}\text{C}$, and a heating rate of 100 $^{\circ}\text{C}/\text{min}$ by sintering in a vacuum environment. The samples were cooled to room temperature and removed from the furnace. All of the sintered samples were subjected to X-ray diffraction (XRD) for phase composition analysis. The density of the alloys was measured by the DX-120Q type densitometer. Hardness was measured by the digital HRS-150 Rockwell hardness tester. Bending strength was tested at room temperature by the AGS-X universal material testing machine; the test samples were 6.5 mm wide and 5 mm thick, with a fixture span of 15 mm and a load rate of 0.05 mm/min. Scanning electron microscopy (SEM) with a S-4800 Type II microscope was used to observe the microstructure of the 90W–6Ni–4Mn alloys.

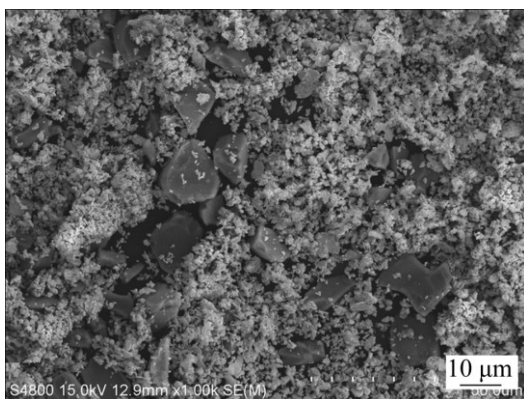


Fig. 1 Morphology of 90W–6Ni–4Mn composite powders

3 Results and discussion

3.1 Densification behavior analysis

The influence of SPS temperature on the relative density of the 90W–6Ni–4Mn alloys is illustrated in Fig. 2. Based on the phase diagram of the alloy composition of 90W–6Ni–4Mn, the temperature of the liquid phase formed by Ni and Mn is 1080 $^{\circ}\text{C}$ [11]. In the solid phase sintering stage, the proliferation and enlargement of internal defects, the interaction of defects, and the formation of new phase caused the preliminary densification. When the sintering temperature was 1050 $^{\circ}\text{C}$, the alloy did not reach the liquid phase point and solid phase sintering was not completed. Consequently, the relative density of the product was low (approximately 71.24%). When the sintering temperature was increased to 1100 $^{\circ}\text{C}$, solid phase sintering was completed and liquid phase sintering was initiated. However, the results achieved at 1100 $^{\circ}\text{C}$ are only slightly higher than those at the liquid phase point of 1080 $^{\circ}\text{C}$. Thus, densification was low and only reached 83.54%. This result showed that the alloy exhibits low densification at a sintering temperature of 1100 $^{\circ}\text{C}$. As the sintering temperature was further increased, the liquid phase was generated. The flow of the liquid phase facilitated the light contact of W grains, whereas the small W particles were dissolved into the binding phase. The dissolving small particles precipitated on the surface of the larger particles by atom diffusion, thereby changing the W grain shape. Later in the sintering process, as part of pore elimination, the grains undergo both size and shape changes by solid dissolution into the liquid, diffusion of that dissolved solid through the liquid, followed by reprecipitation of dissolved solid onto lower energy solid surfaces [12,13]. Thus, spherical W grains with increased densification were formed. The densification of the alloy reached its maximum value of 98.43% at the sintering temperature of 1250 $^{\circ}\text{C}$.

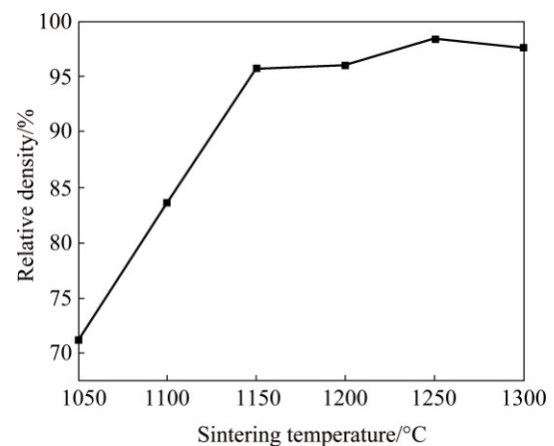


Fig. 2 Relative density as function of sintering temperature for 90W–6Ni–4Mn alloys

3.2 X-ray diffraction analysis

Figure 3 shows the XRD patterns of the 90W–6Ni–4Mn alloys at different sintering temperatures. The main phase of the sintered alloys is the W phase. The W diffraction peak position of the samples does not change significantly at different sintering temperatures. However, the intensity is evidently changed. The Ni and Mn phases do not form a solid solute in the W phase during the sintering process, thereby causing no significant changes in the W diffraction peak position. The intensity of the W diffraction peak gradually increased from 1100 °C to 1200 °C and reached its maximum at 1200 °C. With the further increase in the sintering temperature, the W diffraction peak significantly decreases. This phenomenon is related to the degree of crystallization and grain size. When the sintering temperature was increased, the degree of crystallization further increased and the grains gradually grew. At 1200 °C, the degree of crystallization reached its maximum value, and the alloys exhibited a large grain size. The grain size shows only a slight change after 1200 °C. An increased amount of current is required when sintering temperature is increased to 1250 °C because the instantaneous current fluctuates during sintering. The increased instantaneous current generates high temperature, which satisfies or exceeds the boiling points of Ni and Mn. As a result, some Ni and Mn binding phases evaporate. The alloy is analyzed through energy-dispersive spectroscopy (EDS) with SEM, the results of the analysis are listed in Fig. 4. The figure shows that the Ni and Mn contents decreased after sintering at 1250 °C, thereby resulting in the decrease of intensity of the Ni and Mn diffraction peaks.

3.3 Microstructure evolution of 90W–6Ni–4Mn alloys

The surface morphology of the 90W–6Ni–4Mn alloys under different sintering temperatures is shown in Fig. 5. Simultaneously, the W/W contiguity was

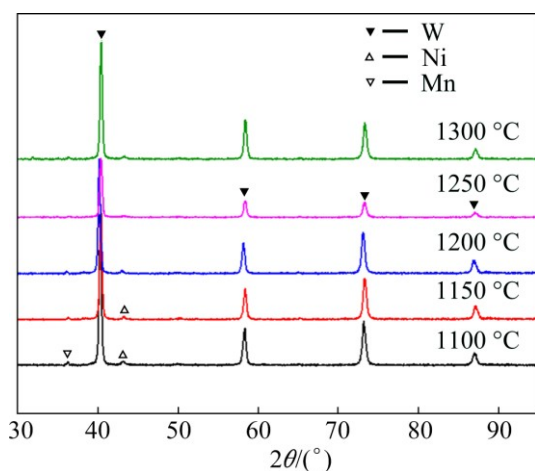


Fig. 3 XRD patterns of 90W–6Ni–4Mn alloys at different sintering temperatures

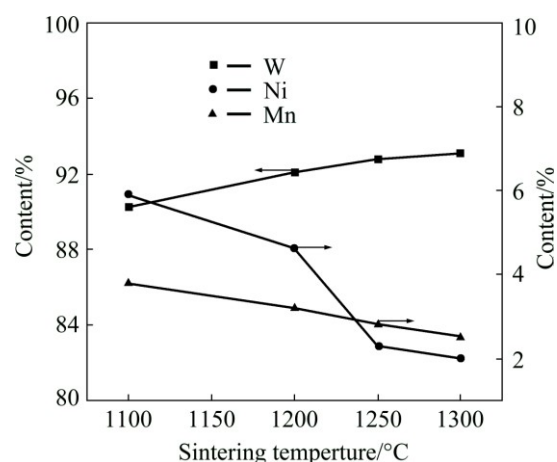


Fig. 4 Chemical compositions of 90W–6Ni–4Mn alloys at different sintering temperatures

measured by using Image-Pro Plus [14] on the basis of the SEM images of the sintered alloy. The results of the W/W contiguity are shown in Table 1. When the sintering temperature was 1050 °C, numerous pores were observed on the surface of the 90W–6Ni–4Mn alloy (Fig. 5(a)). In addition, numerous small W grains were present, and the shape of the W particles was not regular spheres, the W/W contiguity was high. These results were attributed to the sintering temperature, which did not reach the liquid phase point, and the liquid phase sintering of the alloy had not begun. As the sintering temperature increased, the small particles aggregated, and the grain size became larger under the given pressure and temperature (Fig. 5(b)). In Ostwald ripening mechanism, a typical indication of the completion of liquid-phase sintering is the formation of spherical grains. At a sintering temperature of 1100 °C, which exceeds the alloy liquid phase temperature of 1080 °C, the W particles are spherical, as observed in the surface morphological characteristics of 90W–6Ni–4Mn alloys (Fig. 5(b)). This observation indicates that the liquid-phase sintering of the alloy is completed. The average grain size of the alloy is 7 μm and the W/W contiguity decreases. In the previous studies [7], the grain size of the 90W–6Ni–4Mn alloy, which was prepared by vacuum liquid phase sintering, was larger than 10 μm. Compared with other preparation methods, the SPS technique has the following advantages: low sintering temperature, rapid heating rate, and short holding time. Thus, the SPS technique can significantly decrease the size of W grains. When the sintering temperature was increased to 1200 °C, the particle rearrangement and solution–precipitation was overlapping in this stage. The solubility in the liquid phase was related to the size of the W particles. The powders in our experiments were mixed without ball milling; thus, the W particles were larger. However, few W particles are dissolved in the liquid

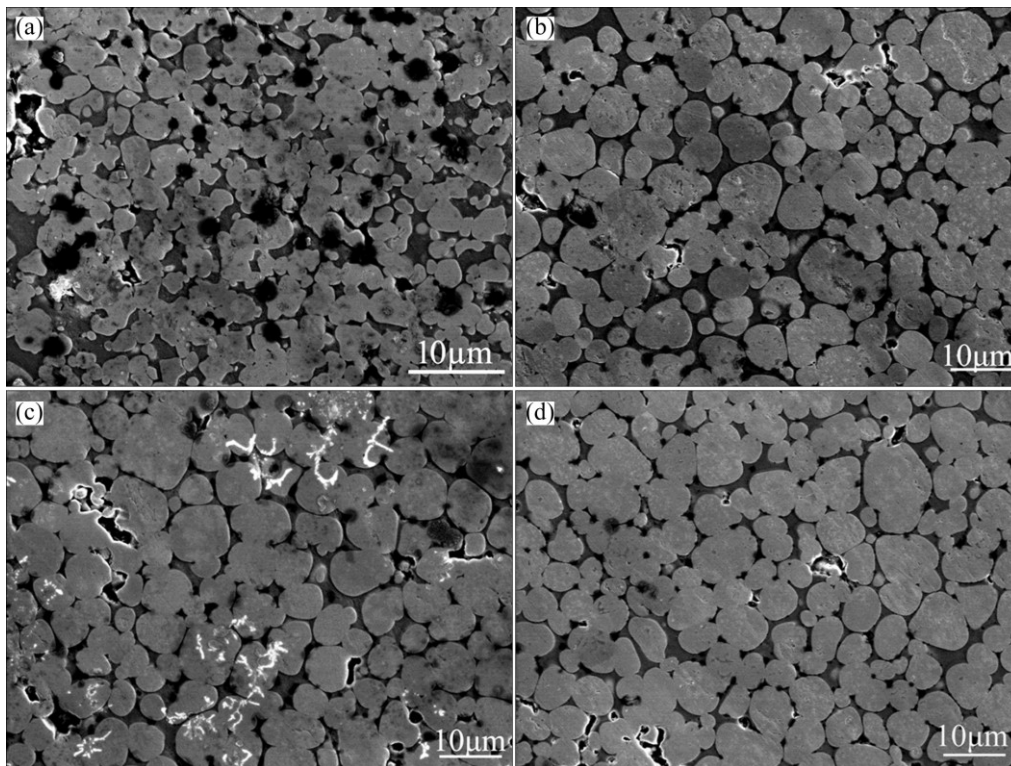


Fig. 5 Surface morphologies of 90W–6Ni–4Mn alloys under different sintering temperatures: (a) 1050 °C; (b) 1100 °C; (c) 1200 °C; (d) 1300 °C

Table 1 W/W contiguity of sintered alloys under different sintering temperatures

Sintering temperature/°C	W/W contiguity/%
1050	77.12
1100	64.33
1200	48.23
1300	50.08

phase. Then the dissolved W particles were diffused in the liquid and re-precipitated onto lower energy solid surfaces, thereby resulting in the W grain growth and shape change (Fig. 5(c)). Meanwhile, the W/W contiguity was further decreased, and the distribution of the binding phase was uniform. With the further increase in the temperature to 1300 °C, the number of connected W grains simultaneously increased (Fig. 5(d)). This phenomenon is related to the volatilization of the binding phase.

The corresponding EDS spectra are shown in Figs. 6(b) and (c). Figure 6(b) shows that Site A in Fig. 6(a) is the W phase and no Ni or Mn solid solutes were observed in the W phase. From Fig. 6(c), Site B is the γ -(Ni, Mn) binding phase, and the W solid solute is in the binding phase. The largest solubility of W (8.86%) in the γ -(Ni, Mn) binding phase in our experiment is lower than that of W (10%–20%) in the γ -(Ni, Fe) binding

phase in a previous study [15], which is decreased to a certain degree. The Ni and Mn are also not dissolved in the W phase. The size of the W particle was large and did not change after homogeneous mixing; thus, only a small quantity of fine W particles was dissolved in the liquid phase, and the content of W in the binding phase was low. However, Ni and Mn easily form the binding phase, and the solubility of the binder metals in W was extremely low. Therefore, Ni and Mn were not readily dissolved into the W phase.

3.4 Mechanical properties of 90W–6Ni–4Mn alloys

The effects of the sintering temperature on the hardness and bending strength of the W alloys are shown in Fig. 7. When the sintering temperature increased, hardness and bending strength first increased and then decreased. When the sintering temperature was increased from 1050 °C to 1150 °C, the hardness increased from HRA 42.6 to HRA 69.1, whereas the bending strength significantly increased from 278.11 MPa to 1108.35 MPa. At lower sintering temperatures, the densification of the sintered alloys was low, and the sintering process continuously occurred with increasing sintering temperature, thereby increasing the densification, hardness, and bending strength of WHAs. This finding corresponds with the densification curve of WHAs shown in Fig. 2. Compared with conventional liquid

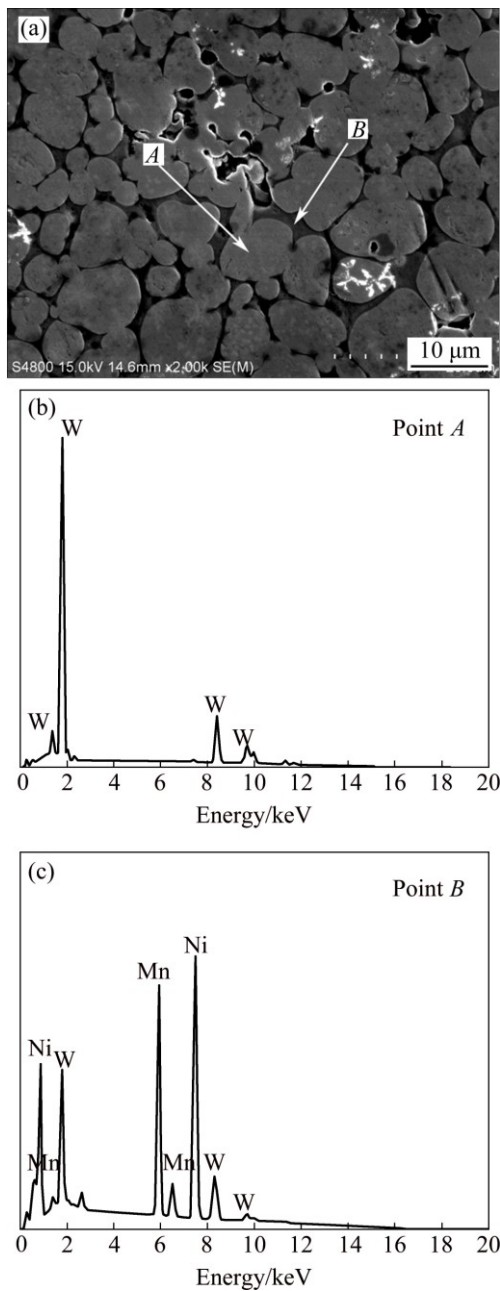


Fig. 6 Microstructure of 90W-6Ni-4Mn alloy sintered by SPS at 1200 °C (a) and EDS spectra (b, c) obtained from Sites A and B shown in (a), respectively

phase sintering, the SPS technique for preparing the W-Ni-Mn alloy uses a lower temperature. Thus, the W particles can form spherical shapes, and the size of the W grains was significantly decreased. Compared with those formed through conventional liquid-phase sintering, the W particles obtained in our proposed sintering method can become spherical because of the effect of Ostwald ripening. Their grain size also significantly decreased because of the very short duration of the proposed sintering (SPS). In conventional sintering, sintering time or the soaking time of sintering is 60–90 min. By comparison, the duration of SPS is 3 min. This result

demonstrates that the duration of solution re-precipitation is not sufficiently long. Consequently, changes in the microstructure and properties (hardness and bending strength) of the alloy were observed. Compared with the W-Ni-Fe alloys [16], W-Ni-Mn alloys did not demonstrate sufficient performance at lower temperatures. The reason is that reduction of Mn oxide in W-Ni-Mn is not easy as reduction of Fe oxide in W-Ni-Fe alloy. Therefore, Mn oxide may exist as an incompletely reduced defect. The densification was lower, and the alloys had numerous pores, which could be regarded as microcracks. These cracks cause stress concentration, which leads to the fracture of the alloys under low stress, thereby decreasing the hardness and bending strength. By increasing the temperature, the sintered W-Ni-Mn alloys demonstrated more sufficient performance, and the densification rapidly increased. These improvements led to the significant improvement of the W-Ni-Mn alloy hardness, which reached similar hardness levels as the W-Ni-Fe alloys at higher temperatures. Further increase in the sintering temperature to 1200 °C allowed the bending strength to reach its maximum value of 1162.72 MPa. With increasing temperature, Ni and Mn reached the theoretical temperatures for the liquid points (the actual temperature may be higher). Consequently, the binding phase was easily formed, and the generation of the binding phase gradually increased. When the sintering temperature exceeded 1250 °C, the evaporation of Ni and Mn increased, thereby reducing the Ni and Mn content, as well as leaving pores in the products. Thus, the hardness and bending strength were decreased.

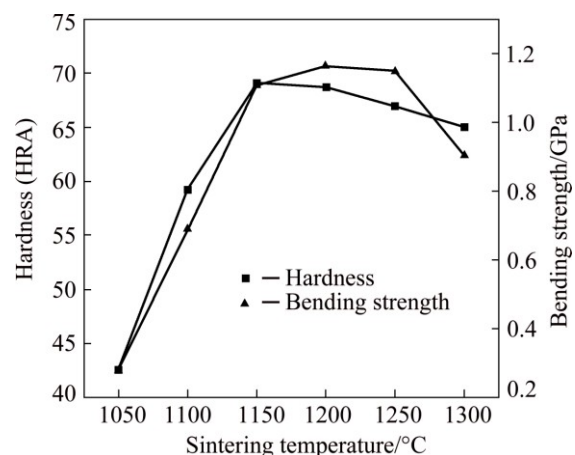


Fig. 7 Hardness and bending strength of 90W-6Ni-4Mn alloys at different sintering temperatures

4 Conclusions

1) The W-Ni-Mn alloys exhibited high densification of 98.43% after preparation by SPS technology at low sintering temperature.

2) As the sintering temperature increased, the densification of the sintered alloys first rapidly increased then slowly further increased before it finally slightly decreased.

3) The hardness and bending strength of the 90W–6Ni–4Mn alloys first increased and then decreased with increasing sintering temperature. The 90W–6Ni–4Mn alloy had the best comprehensive performance at 1200 °C; its hardness and bending strength were HRA 68.7 and 1162.72 MPa, respectively.

4) The 90W–6Ni–4Mn alloy had a small grain size (less than 10 μm). Its microstructure was homogeneous and mainly composed of the W phase and the γ-(Ni, Mn, W) binding phase.

References

- [1] BOSE A, DOWDING R J. Tungsten and tungsten [C]//Proceedings of the first international conference on tungsten and tungsten alloys. Arlington V A. USA: Metal Powder Industries Federation, 1992: 15–22.
- [2] UPADHYAYA A. Processing strategy for consolidating tungsten heavy alloys for ordnance applications [J]. Materials Chemistry & Physics, 2001, 67: 101–110.
- [3] MAGNESS L S. High strain rate deformation behaviors of kinetic energy penetrator materials during ballistic impact [J]. Mechanics of Materials, 1994, 17: 147–154.
- [4] BOSE A, YANG S C, GERMAN R M. Development of a new W–Ni–Mn heavy alloy [J]. Advances in Powder Metallurgy, 1991, 6: 425–437.
- [5] ZAHRAEE S M, ARABI H, SALEHI M T, TAMIZIFAR M. Effect of Mn/Ni ratio variation on microstructure of W–Ni–Mn alloy [J]. Powder Metallurgy, 2008, 51: 303–309.
- [6] LIU H Y, CAO S H, ZHU J, JIN Y, CHEN B H. Densification, microstructure and mechanical properties of 90W–4Ni–6Mn heavy alloy [J]. International Journal of Refractory Metals and Hard Materials, 2013, 37: 121–126.
- [7] CHEN B H, CAO S H, XU H, JIN Y, LI S K, XIAO B. Effect of processing parameters on microstructure and mechanical properties of 90W–6Ni–4Mn heavy alloy [J]. International Journal of Refractory Metals and Hard Materials, 2015, 48: 293–300.
- [8] GUO W Q, LIU J X, LI S K, ZHANG H Y, ZHAO Z Y, CHENG X W. The effect of preparation methods on the microstructure and dynamic compressive properties of 65W–25Cu–10Ni alloys [J]. International Journal of Refractory Metals and Hard Materials, 2015, 48: 238–244.
- [9] GONG X, FAN J L, DING F, SONG M, HUANG B Y. Effect of tungsten content on microstructure and quasi-static tensile fracture characteristics of rapidly hot-extruded W–Ni–Fe alloys [J]. International Journal of Refractory Metals and Hard Materials, 2012, 30(1): 71–77.
- [10] DING L, XIANG D P, LI Y Y, ZHAO Y W, LI J B. Phase, microstructure and properties evolution of fine-grained W–Mo–Ni–Fe alloy during spark plasma sintering [J]. Materials and Design, 2012, 37: 8–12.
- [11] MASSALSKI T B. Binary alloy phase diagrams [M]. Metals Park: ASM International, 1986.
- [12] GERMAN R M. Sintering theory & practice [M]. United States: John Wiley & Sons Inc, 2008: 229–230.
- [13] GERMAN R M. Liquid phase sintering [M]. New York: Plenum Press, 1985.
- [14] AMIRJAN M, ZANGENEH-MADAR K, PARVIN N. Evaluation of microstructure and contiguity of W/Cu composites prepared by coated tungsten powders [J]. Int Journal of Refractory Metals & Hard Materials, 2009, 27(4): 729–733.
- [15] FAN Jing-lian. Tungsten heavy alloy and new fabricating technology [M]. Beijing: Metallurgical Industry Press, 2006. (in Chinese)
- [16] XIANG D P, DING L, LI Y Y, LI J B, LI X Q, LI C. Microstructure and mechanical properties of fine-grained W–7Ni–3Fe heavy alloy by spark plasma sintering [J]. Materials Science and Engineering A, 2012, 551: 95–99.

放电等离子烧结 W–Ni–Mn 合金的 显微组织演变及力学性能

潘艳林, 丁雷, 向道平

海南大学 南海海洋资源利用国家重点实验室, 海口 570228

摘要: 以微米级的钨粉、镍粉和锰粉为原料, 将原料混合均匀后进行放电等离子烧结(SPS)制备 90W–6Ni–4Mn 合金, 探究 SPS 烧结温度对 90W–6Ni–4Mn 合金显微组织演变和力学性能的影响。研究表明, 利用放电等离子烧结(SPS)方法可以在 1150~1250 °C 温度下保温 3 min 制备出近全致密、综合性能优良的 90W–6Ni–4Mn 合金。分析合金显微组织, 90W–6Ni–4Mn 合金组织均匀, 平均晶粒尺寸均在 10 μm 以下, 主要由钨基相和 γ-(Ni, Mn, W)粘结相组成。力学性能测试表明, 提高烧结温度, 合金的洛氏硬度以及抗弯强度均呈先增大后减小的趋势, 在 1200 °C 时其硬度为 HRA 68.7, 抗弯强度达 1162.72 MPa, 综合性能最好。

关键词: 90W–6Ni–4Mn 合金; 放电等离子烧结(SPS); 显微组织; 洛氏硬度; 抗弯强度

(Edited by Yun-bin HE)